JCI insight

Low-dose IL-2 shapes a tolerogenic gut microbiota that improves autoimmunity and gut inflammation

Nicolas Tchitchek,[1] Otriv Nguekap Tchoumba,[1,2] Gabriel Pires,[1] Sarah Dandou,[1] Julien Campagne,[1] Guillaume Churlaud,[1,2] Gwladys Fourcade,[1] Thomas W. Hoffmann,[3,4] Francesco Strozzi,[5] Camille Gaal,[5] Christophe Bonny,[5] Emmanuelle Le Chatelier,[6] Stanislav Dusko Erlich,[6] Harry Sokol,[3,7,8] and David Klatzmann[1,2]

[1]Sorbonne Université, INSERM, Immunology-Immunopathology-Immunotherapy (i3), Paris, France. [2]AP-HP, Hôpital Pitié-Salpêtrière, Biotherapy (CIC-BTi) and Inflammation-Immunopathology-Biotherapy Department (i2B), Paris, France. [3]Micalis Institute, Institut National de la Recherche Agronomique (INRA), AgroParisTech, Univ Paris-Saclay, Jouy-en-Josas, France. [4]Sorbonne University-UPMC Univ Paris 06, INSERM ERL 1157, Avenir Team Gut Microbiota and Immunity, UMR 7203, Paris, France. [5]Enterome, Paris, France. [6]MetaGenoPolis, INRA, Université Paris-Saclay, Jouy-en-Josas, France. [7]Sorbonne Université, Ecole Normale Supérieure, CNRS, INSERM, AP-HP, Laboratoires des Biomolécules (LBM), Paris, France. [8]AP-HP, Hôpital Saint Antoine, Department of Gastroenterology and Inflammation-Immunopathology-Biotherapy Department (i2B), Paris, France.

Gut microbiota dysbiosis is associated with inflammatory bowel diseases and with cardiometabolic, neurological, and autoimmune diseases. Gut microbiota composition has a direct effect on the immune system, and vice versa, and it has a particular effect on Treg homeostasis. Low-dose IL-2 (IL-2$_{LD}$) stimulates Tregs and is a promising treatment for autoimmune and inflammatory diseases. We aimed to evaluate the impact of IL-2$_{LD}$ on gut microbiota and correlatively on the immune system. We used 16S ribosomal RNA profiling and metagenomics to characterize gut microbiota of mice and humans treated or not with IL-2$_{LD}$. We performed fecal microbiota transplantation (FMT) from IL-2$_{LD}$–treated to naive recipient mice and evaluated its effects in models of gut inflammation and diabetes. IL-2$_{LD}$ markedly affected gut microbiota composition in mice and humans. Transfer of an IL-2–tuned microbiota by FMT protected C57BL/6J mice from dextran sulfate sodium–induced colitis and prevented diabetes in NOD mice. Metagenomic analyses highlighted a role for several species affected by IL-2$_{LD}$ and for microbial pathways involved in the biosynthesis of amino acids, short-chain fatty acids, and L-arginine. Our results demonstrate that IL-2$_{LD}$ induced changes in gut microbiota that are involved in the immunoregulatory effects of IL-2$_{LD}$ and suggest a crosstalk between Tregs and gut microbiota. These results provide potentially novel insight for understanding the mode of action of Treg-directed therapies.

Introduction

Autoimmune diseases intrinsically reveal dysregulation of the balance between regulatory and effector immune responses, hence Treg insufficiency (1, 2). Low-dose IL-2 (IL-2$_{LD}$) expands and activates Tregs, and thus has a very broad potential for the treatment of numerous autoimmune, inflammatory, or allergic diseases (2). Furthermore, IL-2$_{LD}$ has pleiotropic effects that can be beneficial in autoimmune diseases, notably the inhibition of the differentiation of naive CD4 cells into proinflammatory Th17 and T follicular helper (Tfh) cells (3, 4). Given that the therapeutic potential of IL-2 is currently being investigated in many autoimmune diseases, understanding its mode of action is of prime importance for rational drug development.

Treg cells are usually defined in humans as CD4⁺Foxp3⁺CD25⁺CD127^{lo} cells, although some Tregs may express a low level of CD25, and as CD4⁺Foxp3⁺ cells in mice. Their main role is to control self-tolerance and inflammation. Indeed, experimental ablation of Tregs immediately triggers severe inflammation, including of the gut, and the development of multiorgan autoimmune diseases (5). Tregs also have important roles in tissue regeneration (6), including in the intestine. IL-2 is the nonredundant key cytokine for the differentiation, survival, and function of Tregs. Mutations of the IL-2 signaling pathway in humans and mice are associated

with systemic inflammation linked to Treg deficiencies (2). Tregs meet their metabolic requirements by utilizing fatty acids and pyruvate oxidation, in contrast to effector T cells, which mainly rely on glycolysis.

The composition of gut microbiota is linked to human health and diseases and is in a dynamic interplay with the immune system (7–10). Gut microbiota composition has a direct effect on the immune environment and vice versa (9, 10). Many factors — including diet (11), environmental exposure (12), and antibiotics (13) — can modify microbiota composition, possibly leading to altered immune homeostasis (14, 15) and secondarily to disease induction. The effects of gut microbiota on immune regulation are in part linked to Treg generation and proliferation in Peyer patches and mesenteric lymph nodes (16, 17). Treg homeostasis in the intestine is mainly controlled by commensal microbial metabolism (18, 19). Tregs from Peyer patches and intestinal mucosa participate in the regulation of intestinal inflammation (20, 21). Thus, as IL-2$_{LD}$ expands and activates Tregs at a systemic but also tissue level, it has the potential to affect gut microbiota composition.

Using 16S ribosomal RNA gene and metagenomic sequencing, we demonstrated that IL-2$_{LD}$ affected gut microbiota composition in mice and humans. Moreover, we showed that gut microbiota from IL-2$_{LD}$–treated animals could be efficiently transplanted to recipient mice that were then protected from gut inflammation and diabetes, demonstrating that the immunoregulatory effects of IL-2$_{LD}$ are in part mediated by gut microbiota modulation.

Results

IL-2$_{LD}$ expands Tregs and protects against autoimmunity and gut inflammation. IL-2$_{LD}$ has been shown to prevent and/or treat numerous autoimmune and inflammatory diseases (2). IL-2$_{LD}$ is defined as a dosage that preferentially stimulates Tregs over effector T cells, which corresponds to doses of around 50,000 IU in mice and around 1 to 3 MIU in humans (2). We investigated the immunoregulatory effects of IL-2$_{LD}$ in an inflammatory colitis model induced by the administration of dextran sulfate sodium (DSS) in the drinking water of C57BL/6J mice. At the time of DSS administration, we treated the mice with IL-2$_{LD}$ intraperitoneal injections daily for 5 days. Such treatment expands and activates Tregs systemically (2), including in the colon (22) and lamina propria (23). It led to significantly lower gut inflammation as evidenced by a much-reduced weight loss (Figure 1A) and disease activity index (Figure 1B) compared with controls.

We also investigated the effects of IL-2$_{LD}$ on the prevention of spontaneous diabetes in NOD mice. In this model, diabetes occurs from around 20 to more than 50 weeks of age according to the experimental conditions, including animal housing. Thus, to obtain a long-term stimulation of Tregs without the need for potentially stressful daily injections, we administered IL-2 by means of a single injection of an IL-2–producing adeno-associated virus (AAV) vector (24) that allows long-term production of IL-2. The dose of vector administered was titrated to obtain Treg activation and expansion similar to what is observed with daily intraperitoneal injections of IL-2$_{LD}$ and without stimulation of effector T cells (24). It is noteworthy that, in the pancreas, this treatment expands Tregs without effects on effector T cells, NK cells, and CD8+ cells (Supplemental Figure 1; supplemental material available online with this article; https://doi.org/10.1172/jci.insight.159406DS1). Thus, under the conditions used, the AAV–IL-2 treatment can be likened to an IL-2$_{LD}$ treatment by daily injections in terms of Treg effects (Figure 1C). As a control for this procedure, we similarly administered a luciferase-producing AAV vector. Control NOD mice had a 60% rate of diabetes occurrence, while those treated with IL-2 were fully protected from diabetes (Figure 1D).

IL-2$_{LD}$ affects gut microbiota composition in mice. To determine whether IL-2$_{LD}$ supplementation induces changes in gut microbiota composition, we first performed 16S rRNA sequencing on feces from 4-week-old NOD and 6-week-old BALB/c mice treated with IL-2 by means of an AAV injection. Because NOD mice have a genetically determined low expression of the *Il-2* gene (25), we hypothesized that this treatment could have a more pronounced effect on their gut microbiota compared with BALB/c mice.

The IL-2$_{LD}$ treatment markedly modified gut microbiota composition in the feces of NOD mice collected on day 30 after the AAV injection. These NOD mice were 8 weeks old at this time point — long before diabetes onset, which did not occur before 20 weeks in our NOD mouse colony. The abundances of 22 taxa were significantly modified in IL-2$_{LD}$–treated NOD mice compared with controls, 13 taxa being upregulated and 9 taxa being downregulated (Figure 2A). The heatmap of the relative abundance of these 22 taxa, combined with unsupervised hierarchical clustering, highlighted that IL-2$_{LD}$ induced modifications in the gut microbiota composition of NOD mice that allowed a perfect separation of IL-2$_{LD}$–treated mice from untreated mice (Figure 2A).
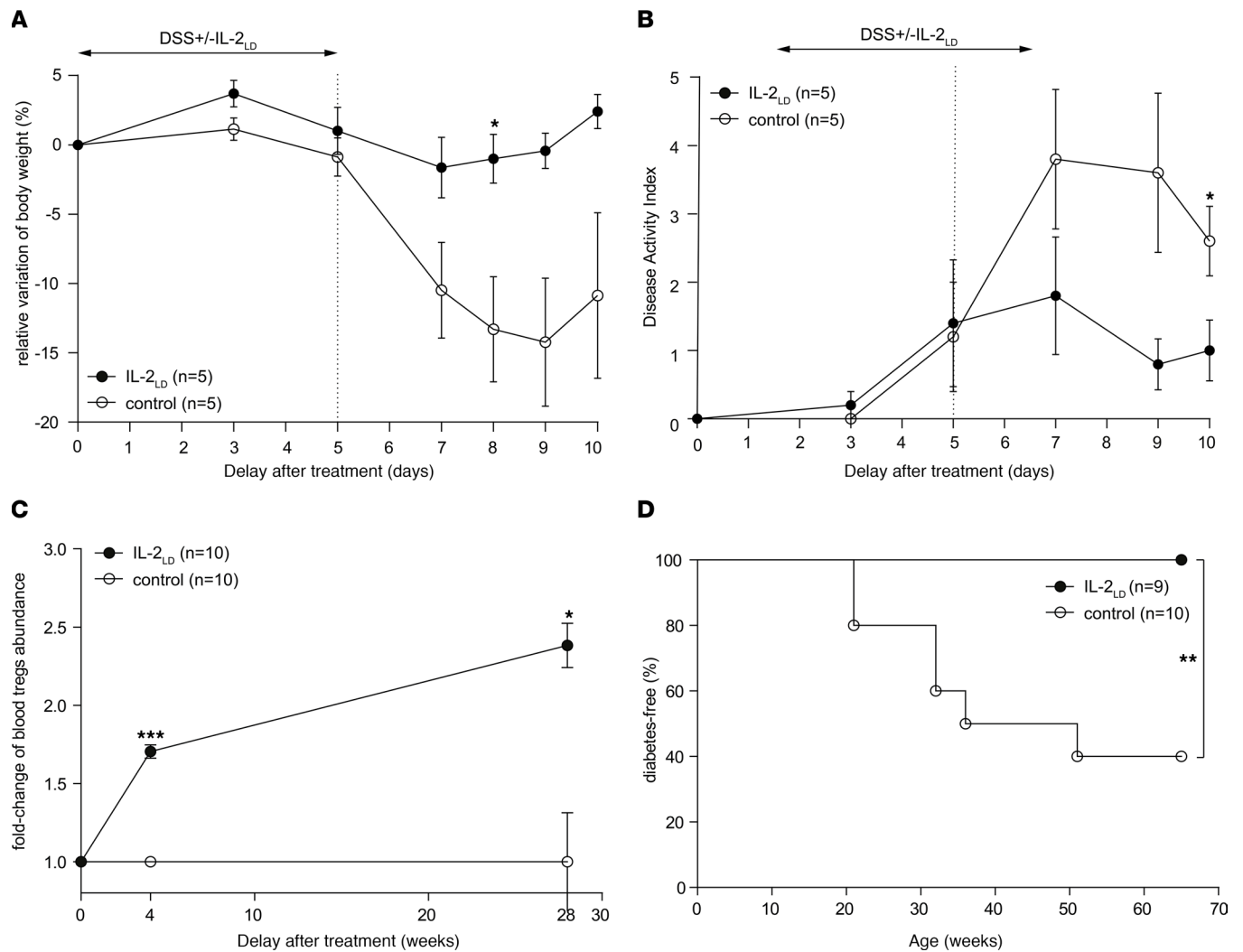
Figure 1. IL-2$_{LD}$ protects from autoimmunity. (A and B) C57BL/6J female mice were treated or not with IL-2$_{LD}$ by means of intraperitoneal injections of IL-2 during 5 consecutive days. Dextran sulfate sodium (DSS) was administered in drinking water during the same 5 days. The body weight measurements expressed as percentages relative to baseline (**A**) and the colitis disease activity index (**B**) were evaluated at baseline and thereafter. (**C and D**) NOD female mice were treated or not with IL-2$_{LD}$ by means of IL-2–producing or luciferase-producing AAV vectors. (**C**) Fold changes of blood Tregs at baseline and after treatment. (**D**) Kaplan-Meier estimators of diabetes onset in NOD mice. Two-tailed Student's t test was used to compare measurements in treated and untreated mice at each time point. The χ^2 test was used to compare the Kaplan-Meier estimators. The Holm-Bonferroni adjustment was used for multiple-comparison correction. Statistical significances are denoted as follows: *$P < 0.05$; **$P < 0.01$; ***$P < 0.001$. For each biological condition, the total number of mice used is provided in parentheses.

As hypothesized, the gut microbiota composition was less affected by the IL-2$_{LD}$ treatment in BALB/c mice. Only 4 taxa were significantly modified in IL-2$_{LD}$–treated mice compared with controls (Figure 2B). In line with this observation, the heatmap of relative taxa abundances combined with unsupervised hierarchical clustering outlined that IL-2$_{LD}$ induced gut microbiota modifications that did not allow a perfect separation of IL-2$_{LD}$–treated mice from untreated mice (Figure 2B).

These differences between the changes in microbiota induced by IL-2$_{LD}$ in NOD and BALB/c mice prompted us to compare their gut microbiota composition before treatment. We observed remarkable differences for these mice raised in the same animal facility and fed with the same chow (Figure 2C). A heatmap of relative taxa abundances combined with unsupervised hierarchical clustering allowed a perfect separation of NOD and BALB/c mice (Figure 2C). Among the 22 taxa dysregulated by IL-2$_{LD}$ in NOD mice, *Intestinimonas* was enriched in BALB/c compared with NOD mice and was enriched by IL-2$_{LD}$ in NOD mice. Reciprocally, *Parasutterella*, *Ruminococcaceae UCG−013*, and *ASF356* were less represented in BALB/c compared with NOD mice and were reduced by IL-2$_{LD}$ in NOD mice (Supplemental Figure 2).
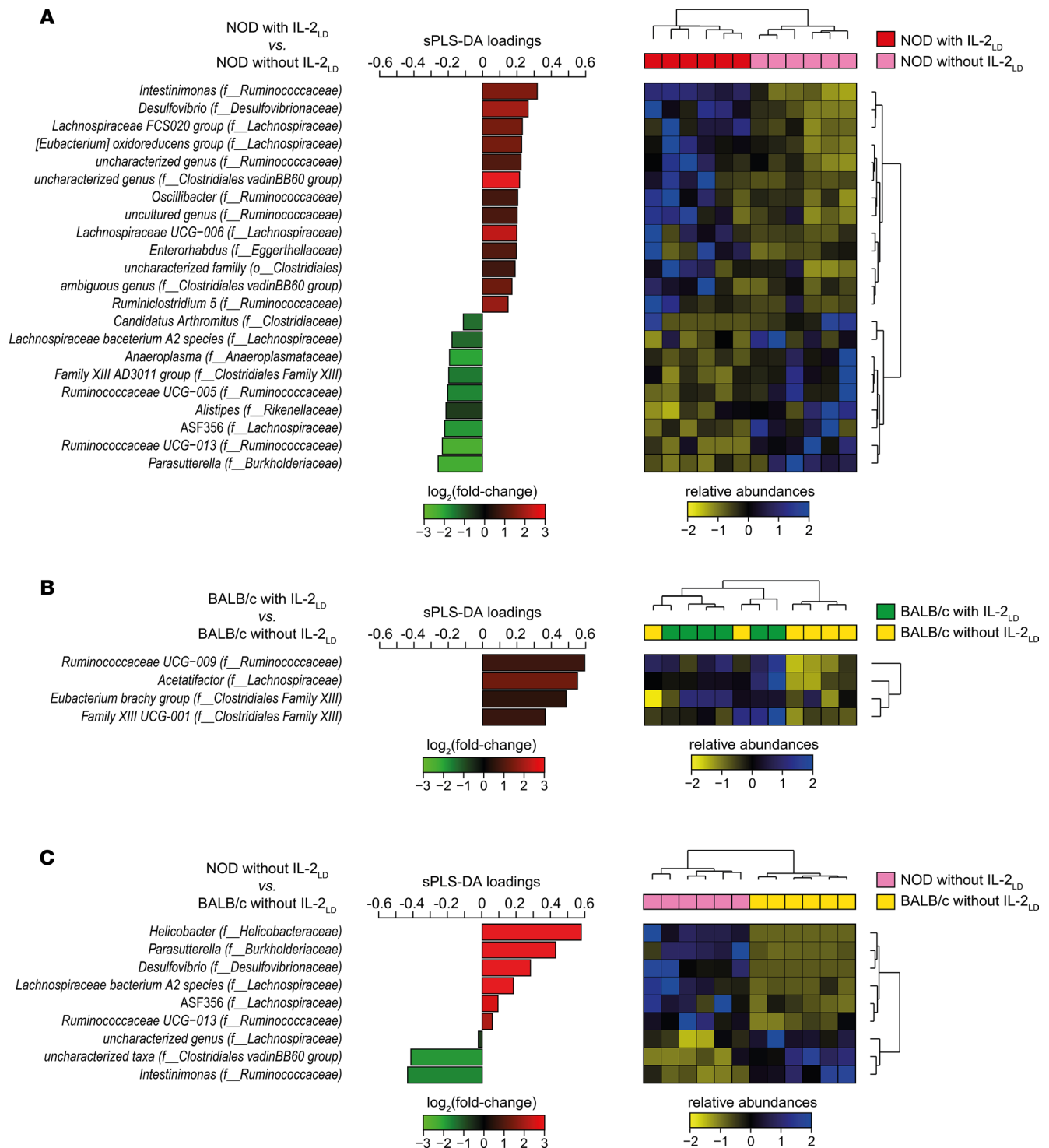
Figure 2. IL-2_LD affects gut microbiota composition in mice. NOD and BALB/c mice were treated or not with IL-2_LD by means of IL-2–producing or lucif-erase-producing AAV vectors. Profiling of their gut microbiota, collected 30 days after treatment, was performed using 16S rRNA sequencing. (**A** and **B**) Comparisons were made between NOD mice and BALB/c mice treated or not with IL-2_LD. (**C**) An additional comparison was made between NOD mice and BALB/c mice without IL-2_LD to comprehend the gut microbial specificities associated with these mouse backgrounds. For each comparison, sPLS-DA was conducted to identify the gut microbial taxa best able to discriminate the conditions. The contribution of each taxon identified by sPLS-DA was represented using a horizontal bar of length proportional to its sPLS-DA loading. Horizontal bars were gradient-colored based on the $\log_2$ of the taxa abundance fold-changes relative to the reference group. For each analysis, a heatmap of relative abundances combined with unsupervised hierarchical clustering was used to evaluate the capacity of the list of taxa to discriminate the conditions. The family (f__) or order (o__) associated with the taxa identified by sPLS-DA is indicated in parentheses.

Thus, IL-2$_{LD}$ treatment, which confers protection against autoimmunity, was associated with gut microbiota changes in two distinct genetic backgrounds. Moreover, the gut microbiota of NOD mice, which have a genetically determined low IL-2 production (25), was the more affected.

IL-2$_{LD}$–tuned gut microbiota can be transplanted and confer protection from autoimmunity and gut inflammation. Given that IL-2$_{LD}$ modifies gut microbiota composition, which is in interplay with the immune system, we hypothesized that an IL-2$_{LD}$–tuned microbiota could participate in the immunoregulatory effects of IL-2$_{LD}$. We first verified that we could indeed transplant an IL-2$_{LD}$–tuned microbiota to naive mice (so-called IL-2$_{LD}$–tuned fecal microbiota transplantation [FMT]). NOD mice were treated with IL-2–producing or luciferase-producing AAV vectors, and their gut microbiota were collected 30 days thereafter. Collected microbiota were orally transferred in 2 groups of 6-week-old recipient NOD mice whose gut microbiota had been cleared with a cocktail of antibiotics (ATB) during the 14 days preceding FMT. 16S rRNA sequencing was performed on the recipient NOD mice after transplantation with IL-2$_{LD}$–tuned FMT or with control FMT. Multidimensional scaling representation of gut microbiota composition showed that the microbiota from IL-2–treated NOD donors could be efficiently transplanted, as it was similar to that of recipient mice (Supplemental Figure 3). Furthermore, as shown in Figure 3A, 18 taxa were significantly different between recipients of gut microbiota from IL-2$_{LD}$–treated or control NOD mice (i.e., after FMT). A heatmap of relative taxa abundances combined with hierarchical clustering showed a perfect separation between NOD mice transplanted with an IL-2$_{LD}$–tuned or control gut microbiota. Six taxa were affected by both IL-2$_{LD}$ treatment and IL-2$_{LD}$–tuned FMT in NOD mice (Figure 3B). Of these, *Desulfovibrio,* the *Lachnospiraceae bacterium A2* species, an uncultured genus of the *Ruminococcaceae* family, and an uncharacterized genus of the *Clostridiales vadinBB60 group* family were upregulated or downregulated in a concordant manner in the 2 conditions.

Because an IL-2$_{LD}$–tuned microbiota can be engrafted, we tested whether a transferred IL-2$_{LD}$–tuned microbiota could confer some protection against autoimmunity and gut inflammation. An IL-2$_{LD}$–tuned microbiota FMT did indeed significantly protect C57BL/6J mice from colitis induced by DSS. Weight loss (Figure 3C) and disease activity index (Figure 3D) were markedly and significantly reduced compared with untreated mice, to mice that received control FMT, and to mice treated with ATB. The mice having received ATB and no FMT behaved as the untreated control mice. This is not surprising because the colitis was induced 2 weeks after the ATB treatment, which left time for microbiota reconstitution.

Similarly, NOD mice that received IL-2$_{LD}$–tuned microbiota had a reduction of diabetes incidence compared with mice that received control FMT in the 50 weeks after treatment (Figure 3E).

Altogether, these results showed that an IL-2$_{LD}$–tuned microbiota could be efficiently transplanted to IL-2–naive recipient mice and protected against autoimmunity and gut inflammation in 2 murine genetic backgrounds. These results prompted us to analyze further the effects of IL-2 on gut microbiota by shotgun metagenomic sequencing.

Identification of microbiota species affected by IL-2$_{LD}$. To further characterize the changes in gut microbiota composition induced by IL-2$_{LD}$, we performed gut microbiome profiling from IL-2$_{LD}$–treated NOD and C57BL/6J mice using shotgun metagenomics. The Simka algorithm was first used to quantify the effects of the IL-2 treatment between profiles without defining a prior metagenome reference (26).

Clustering based on the Jaccard distance perfectly separated NOD and C57BL/6J mice, and within these clusters, separated the IL-2$_{LD}$–treated mice from the untreated mice (Figure 4A), indicating that the NOD microbiota still differed from that of C57BL/6J mice after IL-2$_{LD}$ treatment. We found that 13 taxa were dysregulated by IL-2$_{LD}$ in C57BL/6J mice and 17 were dysregulated in NOD mice, with 8 species simultaneously affected in the 2 mouse backgrounds (Figure 4B). *Akkermansia muciniphila* was upregulated by IL-2$_{LD}$ in both mouse backgrounds. *Lactobacillus gasseri*, *Lactobacillus johnsonii*, and *Lactobacillus reuteri* were downregulated by IL-2$_{LD}$ in both mouse backgrounds. Additionally, *Alistipes unclassified*, *E. coli*, *Escherichia unclassified*, and *Parabacteroides goldsteinii* were dysregulated by IL-2$_{LD}$ but with different directionalities.

Principal component analysis based on abundances clearly showed a strong effect of IL-2$_{LD}$ in both genetic backgrounds (Figure 4, C and D). It is noteworthy that these results were reproduced using an independent computational analysis (Supplemental Figure 4, A and B).

Identification of microbial functional pathways affected by IL-2$_{LD}$. We next performed a functional analysis to gain more insight into microbial changes affected by the IL-2$_{LD}$ treatment. We found that IL-2$_{LD}$ affected 210 pathways in C57BL/6J mice and 92 pathways in NOD mice. Heatmaps of relative pathway abundances combined with hierarchical clustering showed a perfect separation between treated and untreated mice in both genetic backgrounds (Figure 5, A and B).
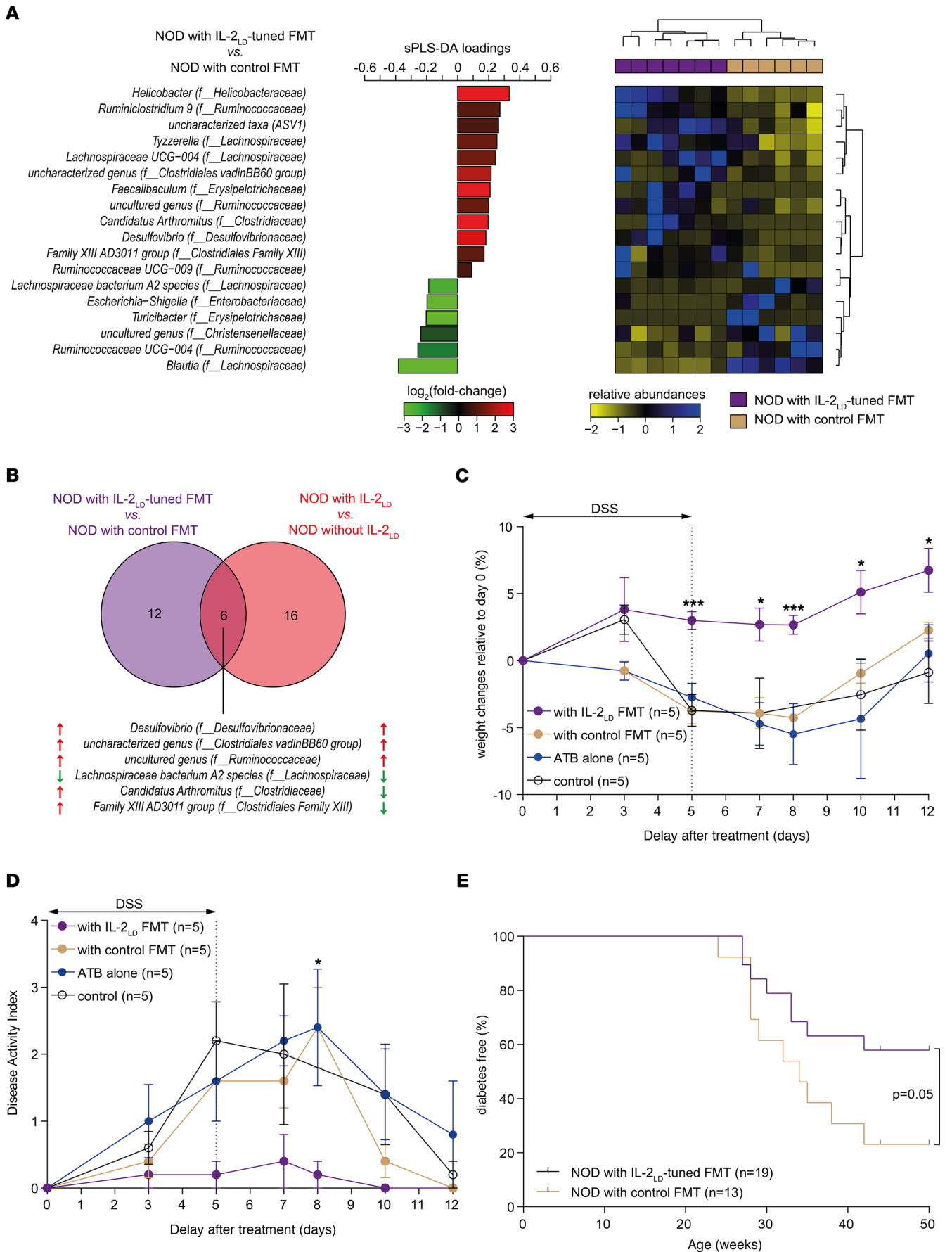
Figure 3. IL-2$_{LD}$–tuned gut microbiota protects from autoimmunity. The microbiota of IL-2$_{LD}$–treated NOD mice was transferred to recipient NOD mice treated by antibiotics (ATB) for 14 days before fecal microbiota transplantation (FMT). NOD mice receiving FMT from untreated NOD mice were used as controls. 16S rRNA sequencing was used to profile gut microbiota at day 30 after treatment. (**A**) sPLS-DA was conducted to identify taxa separating NOD mice with FMT IL-2$_{LD}$ from NOD mice with control FMT. The contribution of each taxon identified by sPLS-DA was represented using a horizontal bar of length proportional to its sPLS-DA loading. A heatmap of relative abundances combined with unsupervised hierarchical clustering was used to evaluate the capacity of the list of taxa to discriminate the conditions. (**B**) Venn diagram showing the overlap between the lists of taxa affected by IL-2$_{LD}$ and IL-2$_{LD}$ FMT treatments relative to their control groups. (**C** and **D**) In an independent experiment, C57BL/6J mice were treated with IL-2$_{LD}$. Five weeks later, fresh stools from these mice were collected and orally administered to 7-week-old female C57BL/6 mice previously treated daily for 14 days with ATB. DSS was administered in drinking water for 5 days after transplantation to trigger colitis. Mouse body weight change (**C**) and disease activity index (**D**) were evaluated until day 12. (**E**) In an independent experiment, 4-week-old female NOD mice were treated with IL-2$_{LD}$ or without IL-2$_{LD}$. Five weeks later, fresh stools from these mice were collected and orally administered to 6-week-old female NOD mice previously treated daily for 14 days with ATB. Diabetes onset was screened for during the experiment. Student's *t* test was used to compare measurements in treated and untreated mice at each time point. The Holm-Bonferroni adjustment was used for multiple-comparison correction. Statistical significances were reported as follows: *$P < 0.05$; ***$P < 0.001$. IL-2$_{LD}$ was administered or not to mice by means of IL-2–producing AAV. For each biological condition, the total number of mice used is provided in parentheses.

A total of 17 pathways were concordantly upregulated or downregulated in both C57BL/6J and NOD mice relative to their respective untreated controls (Figure 5C). These pathways were mainly associated with biosynthesis, energy metabolism, and glycan mechanisms — including L-arginine biosynthesis and inosine 5 phosphate biosynthesis — with many species contributing to these changes.

Overall, these results indicated that IL-2$_{LD}$–induced modifications in microbial populations profoundly affected pathways that could affect interaction with immune cells.

IL-2$_{LD}$ treatment affects the microbiome of patients with autoimmune diseases. We next assessed whether IL-2$_{LD}$ also influences gut microbiota in humans. We performed metagenomics profiling of feces samples from 6 patients with autoimmune diseases treated by IL-2$_{LD}$ (TRANSREG trial, ClinicalTrials.gov NCT01988506) (27). Feces were collected at baseline and between 3 and 6 months after treatment initiation.

We found 5 bacterial species affected by IL-2$_{LD}$ in patients (Figure 6A). At the functional level, we found 63 microbial pathways affected by IL-2$_{LD}$ in patients, all of them being downregulated in samples obtained after IL-2$_{LD}$ treatment relative to the respective baseline samples (Figure 6B). These pathways were mainly associated with nucleotide biosynthesis, biosynthesis, cofactor biosynthesis, amino acid biosynthesis, and degradation (Figure 6C). For each of these pathways, we quantified the number of associated bacterial species (i.e., the number of species expressing each given pathway). We found that the adenosine ribonucleotide de novo biosynthesis, super pathway of coenzyme A biosynthesis III, 5-aminoimidazole ribonucleotide biosynthesis I, UMP biosynthesis I, and methylerythritol phosphate pathways had the highest numbers of associated species (>80). L-arginine biosynthesis was also found to be affected by IL-2$_{LD}$ with multiple pathways having high numbers of associated species.

The 6 patients' pre– and post–IL-2LD gut microbiota samples clustered well together, as shown by the heatmaps of relative taxa abundances (Figure 6A) or pathways (Figure 6B) combined with unsupervised hierarchical clustering.

Discussion

We demonstrated here that IL-2 shaped gut microbiota, at both the taxonomic and functional levels, in 3 murine genetic backgrounds and in patients with autoimmune diseases. Moreover, we showed that IL-2–tuned microbiota could be transplanted and protected IL-2–naive recipient mice against experimental inflammatory bowel disease and diabetes.

IL-2$_{LD}$ shapes fecal microbiota in different species. Gut microbiota has the potential to shape the immune system (19, 28). In return, the immune system can have an impact on gut microbiota. Recently, modulation of expression of IL-17, a proinflammatory cytokine that contributes to both autoimmunity and host immune defense, has been reported to induce modifications of gut microbiota (29) that led to protection against central nervous system autoimmunity. Mirroring these observations, we showed that a cytokine that expands and activates Tregs also shaped gut microbiota composition in 3 mouse genetic backgrounds and in humans. In mice, principal component analysis and hierarchical clustering perfectly separated the microbiota of IL-2–treated versus control mice in the 3 genetic backgrounds, using 2 independent taxonomic profiling methods. Interestingly, the number of microbial taxa that changed after IL-2$_{LD}$ was always higher in NOD mice than in BALB/c or in C57BL/6J mice. Because NOD mice have genetically controlled low IL-2 production that leads to Treg deficiency (25), this emphasizes the importance of the gut microbiota/IL-2/Treg axis in health and disease. Our results extend the recent observation that IL-2 leads
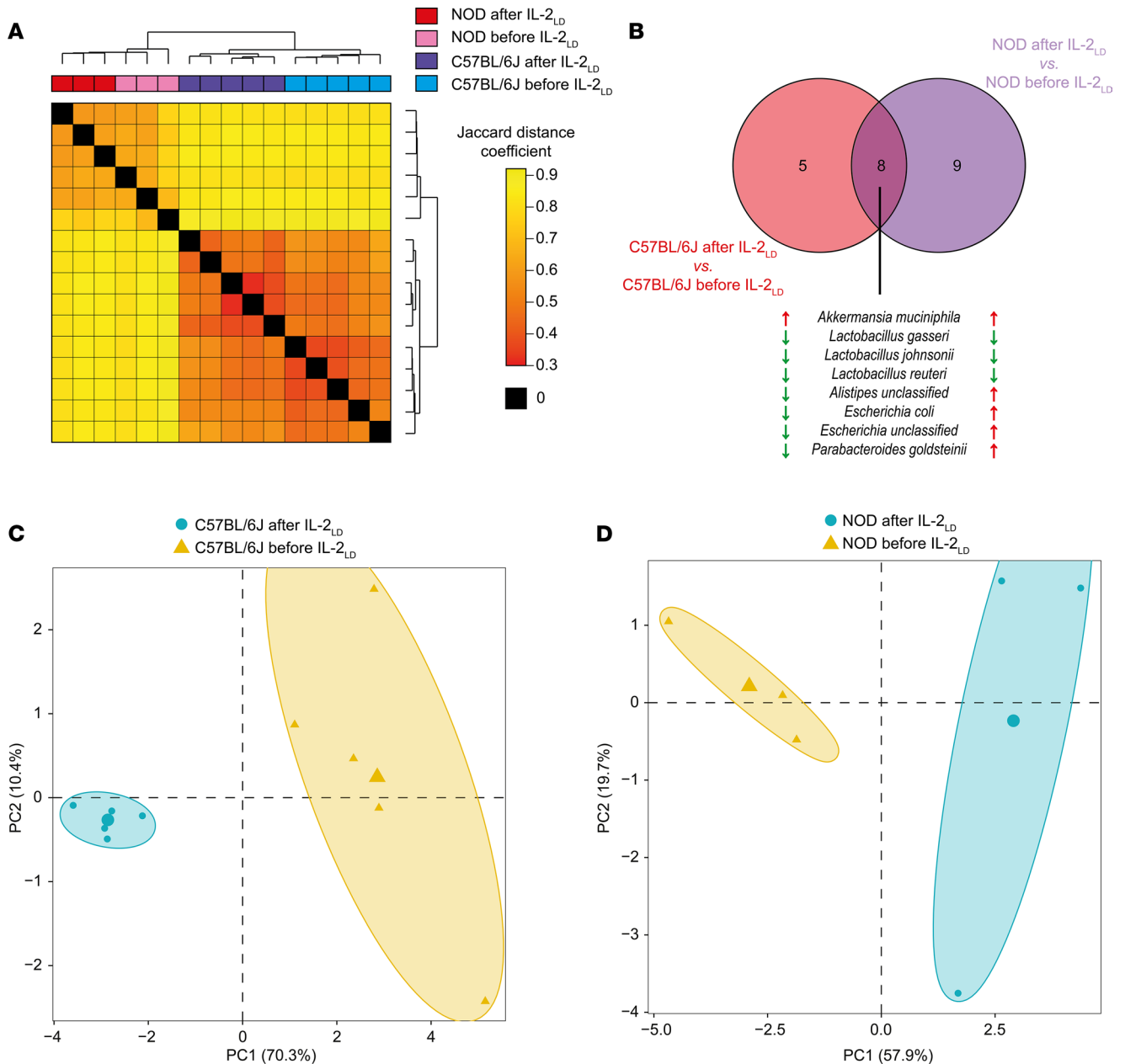
Figure 4. Metagenomics reveals microbial species affected by IL-2$_{LD}$. To gain more insight into the impact of IL-2$_{LD}$ on microbial composition, gut micro-biome profiling of NOD and C57BL/6J mice before and 30 days after IL-2$_{LD}$ treatment was performed using metagenomics. (**A**) Distogram representation showing the distance between microbiome profiles. Similarities were calculated using the Simka algorithm, which compares profiles using a k-mer approach without needing a reference metagenome, and using the Jaccard distance coefficient on abundance levels. (**B**) Venn diagram showing the overlap between the lists of taxa significantly affected by IL-2$_{LD}$ in NOD and C57BL/6J mice. The names of the overlapping species are indicated, and their upregu-lation and downregulation relative to controls are respectively indicated by red or green arrows. (**C** and **D**) Principal component analysis representations of the gut microbiome profiles of NOD and C57BL/6J mice before and after treatment with IL-2$_{LD}$ generated using the abundance levels of taxa significantly affected by IL-2$_{LD}$. IL-2$_{LD}$ was administered to mice by means of an IL-2–producing AAV vector.

to modification of gut microbiota in NOD mice using 16S rRNA analysis (23). Here, we extend this work by showing that IL-2–tuned microbiota had an immunoregulatory effect and by analyzing IL-2–treated patients. We observed a clear impact of IL-2$_{LD}$ on the microbiome in humans, although this impact was less pronounced than that observed in mice, likely because of higher interindividual variability. Neverthe-less, as for mice, we could accurately cluster together the pre–IL-2$_{LD}$ gut microbiota and post–IL-2$_{LD}$ gut microbiota from these patients. This is remarkable. Indeed, given that diet as well as disease conditions profoundly affect gut microbiota composition, it could have been expected that pre– and post–IL-2$_{LD}$
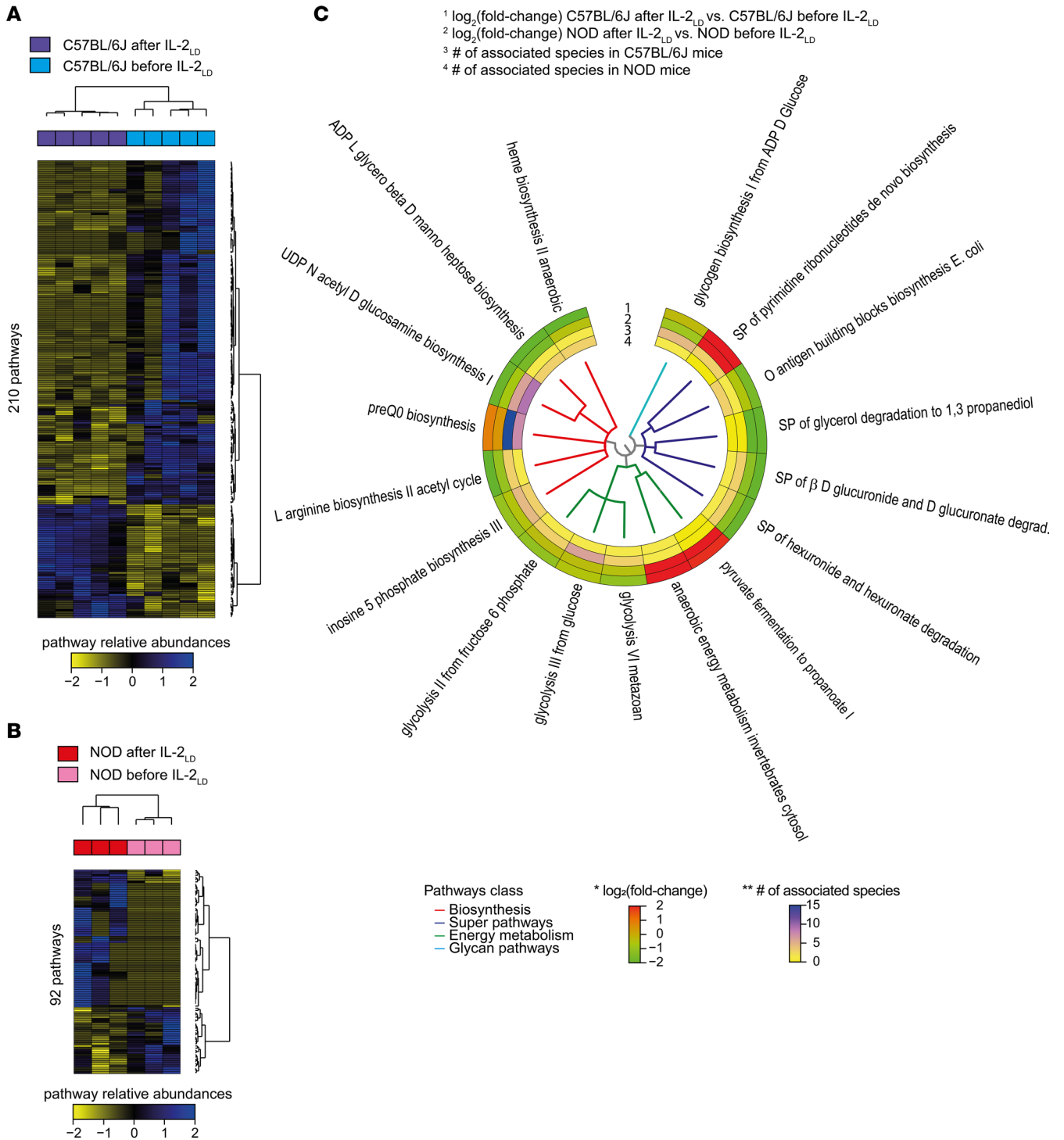
Figure 5. Metagenomics reveals microbial pathways affected by IL-2_LD. (**A** and **B**) Heatmap representations combined with unsupervised hierarchical clustering of relative abundance levels for microbial pathways affected by the IL-2_LD treatment in C57BL/6J and NOD mice relative to their baseline conditions. (**C**) Circular tree representation using color-gradient scales showing the fold-change of microbial pathway abundances and the number of species associated for the 17 pathways affected by IL-2_LD in C57BL/6J and NOD mice and with the same directionality. The classes of each pathway are also indicated in different colors. The * symbol indicates the log_2 of the fold changes of microbial pathway abundances using a color-gradient scale ranging from green to red. The ** symbol indicates the number of associated species to each pathway using a color-gradient scale ranging from yellow to blue. IL-2_LD was administered to mice by means of an IL-2–producing AAV vector.
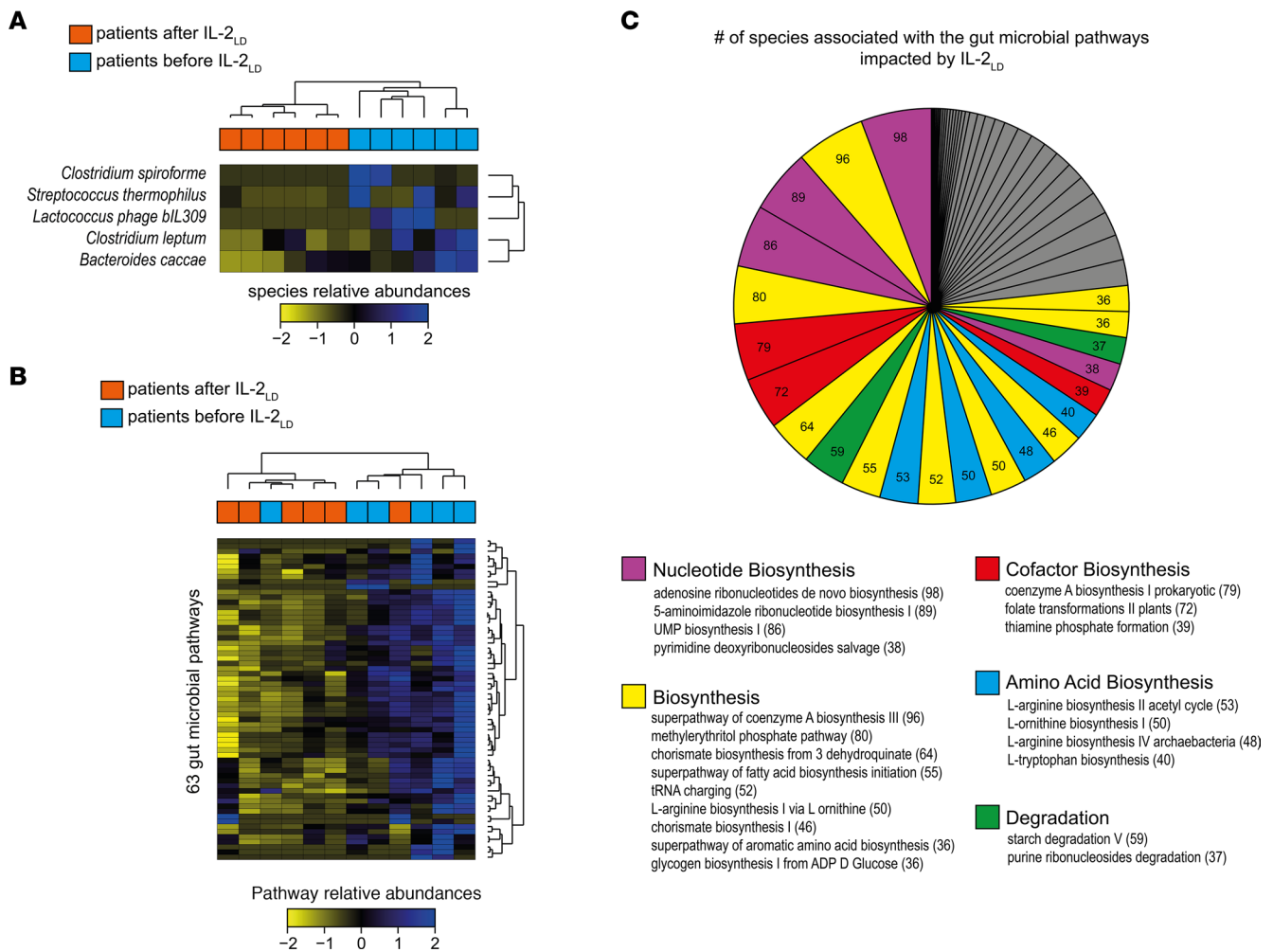
Figure 6. IL-2$_{LD}$ affects the gut microbiome in patients with autoimmune disorders. To evaluate the potential of IL-2$_{LD}$ to modify the gut microbiome in humans, 6 patients with various autoimmune diseases were treated with IL-2$_{LD}$. Samples were collected at baseline and between 3 and 9 months after the first injection. Microbiome profiling was performed using metagenomics. (**A**) Heatmap representation of the relative abundances for the 5 bacterial species found to be differentially abundant in the gut microbiome of patients treated with IL-2$_{LD}$ relative to the baseline condition. (**B**) Heatmap representation of relative abundances for the 63 microbial pathways found to be differentially abundant in the gut microbiome of patients. (**C**) Pie chart showing the number of taxa associated with the microbial pathways differentially abundant in patients relative to baseline. Gut microbial pathways are colored according to their classes. The number of contributing species is indicated in parentheses for each pathway. Pathways with fewer than 36 associated taxa are colored in gray.

treatment samples from a given patient would have clustered together. Thus, based on the differentially abundant taxa and pathways, the robustness of the gut microbiota changes induced by IL-2$_{LD}$ in humans was more discriminating than the individual's gut microbiota composition.

IL-2 licenses the gut microbiota to act as an immunomodulatory drug. The bidirectional interdependency of the gut microbiota and the immune system has raised the possibility that gut microbiota could modulate/mediate the efficacy of immunotherapies, which has indeed been observed for cancer immunotherapies (30–32). Here, we report the ability of an immunomodulatory treatment targeting Tregs to confer its immunoregulatory potential on gut microbiota.

This is important because alternatives to IL-2–producing AAV or IL-2 intraperitoneal injections have now been developed to stimulate Tregs. Among them is the use of IL-2 complexes with enhanced specificity for Tregs (33) or the use of the superagonistic anti-CD28 antibody (34). The impact of these Treg stimulation methods on the gut microbiome has yet to be studied.

Note that IL-2–tuned FMT resulted in control of 2 independent disease conditions, like the IL-2$_{LD}$ treatment itself. Thus, IL-2$_{LD}$ not only changed the composition of intestinal microbial taxa, but also licensed microbiota to act as an immunomodulatory treatment. This opens the interesting possibility of manipulating the microbiota before its transplantation, so as to improve its efficacy.

Gut microbiota modifications induced by IL-2 are relevant for the immunomodulatory effect of IL-2$_{LD}$–tuned microbiota. Our gut microbiota profiling provides some insights into the potential mechanisms by which IL-2$_{LD}$ may affect the host. First, the majority of taxa differentially expressed in IL-2$_{LD}$–treated NOD mice belong to the *Ruminococcaceae* family. Members of this family have been reported to be decreased in many autoimmune or inflammatory diseases, notably in patients with type 1 diabetes or Crohn's disease (35, 36). Second, taxa of *Intestinimonas*, the most differentially abundant genus in IL-2$_{LD}$–treated-NOD mice compared with controls, have been reported to be decreased in patients with type 1 diabetes (35). *Intestinimonas* are also known to be producers of short-chain fatty acids, which are known to promote immunomodulation by favoring Tregs and limiting effector T cells (37–39). Third, *Akkermansia muciniphila* is increased by IL-2$_{LD}$ treatment in NOD and C57BL/6J mice and is more differentially abundant in IL-2–treated NOD mice than in IL-2–treated C57BL/6J mice. This taxon a) has been described as a protector against autoimmunity in NOD mice and against DSS-induced colitis, and b) can also promote Tregs in inflammatory bowel diseases in mice (40, 41). Furthermore, the abundance of *Akkermansia muciniphila* has been shown to be associated with Treg proliferation (42). Fourth, Rowan et al. found that *Desulfovibrio* was significantly increased in acute and chronic human ulcerative colitis (43). Here, we found that this species was increased in IL-2$_{LD}$–treated NOD mice compared with untreated NOD mice, as well as in NOD mice with IL-2$_{LD}$–tuned FMT compared with NOD mice with control FMT. Additionally, the *Desulfovibrio species* was found to be upregulated in untreated NOD mice relative to untreated BALB/c mice.

Together, these observations point to a crosstalk between Tregs and these taxa that could provide at least part of the mechanism driving the immunoregulatory efficacy of FMT of IL-2–tuned microbiota.

Downstream of the modifications of taxa composition by IL-2$_{LD}$, we also identified functional pathways that could participate in the immunoregulatory efficacy of IL-2–tuned microbiota. We identified a core of 17 microbial metabolic pathways that changed in both NOD and C57BL/6J mice after this IL-2$_{LD}$ treatment. The biosynthesis of L-arginine, an amino acid described as a fuel for the generation of citrullinated peptides that could trigger autoimmune responses, notably in type 1 diabetes (44–46), is decreased in intestinal microbes of IL-2$_{LD}$–treated mice and humans. Conversely, metabolic pathways leading to the increase of short-chain fatty acids (e.g., pyruvate fermentation to propanoate I) were increased by IL-2$_{LD}$ treatment in both murine genetic backgrounds. This observation is in line with our previous comment related to the major increase in *Intestinimonas,* known as short-chain fatty acid producers, in IL-2$_{LD}$–treated NOD mice. With the recent report that FMT from healthy donors halts the progression of new-onset type 1 diabetes in humans (47), our results suggest that the use of IL-2–tuned FMT or of FMT enriched in specific taxa could represent an improved treatment modality.

In summary, gut microbiota modifications induced by IL-2$_{LD}$ appear to favor taxa and microbe metabolic pathways that influence the Treg/effector T cell balance. Our results call for extended studies in human cohorts to confirm our observations. Our work suggests a virtuous circle in which IL-2$_{LD}$ affects gut microbiota, and in return gut microbiota reinforces the primary effect of IL-2$_{LD}$ on Treg/effector T cell balance. It should be noted that Tregs can shape gut microbiota (48), and it is also known that IL-2$_{LD}$ directly affects Tregs. Thus, we can postulate that IL-2 may affect gut microbiota through the modulation of Tregs. This has implications for a better understanding of how gut microbiota participates in and maintains disease conditions and for the better design of immunoregulatory therapies, including improved FMT.

The fact that IL-2–tuned microbiota act as an immunomodulatory treatment opens the possibility to manipulate gut microbiota for improved FMT and to discover microbial-derived molecules to treat autoimmune and inflammatory diseases. The effects of IL-2$_{LD}$–tuned FMT on the recipient immune system, notably at the level of the T cell receptor (TCR) repertoire of Tregs, have yet to be evaluated.

Methods

Housing of mice and ethical statements. Female BALB/c mice, C57BL/6J mice, NOD mice, and NOD mice expressing GFP under the control Foxp3 gene promoter were maintained under pathogen-free conditions according to European legislation. All mice received the same food, which was normal-protein chow.

Administration of IL-2$_{LD}$. IL-2$_{LD}$ was administered either a) by a single injection of an IL-2–producing recombinant AAV vector serotype 8 (AAV8) (rAAV) vector and compared with the injection of a luciferase-producing control rAAV, both at a concentration of 10^{10} rAAV viral genomes as previously

described (24); or b) by intraperitoneal injections with 50,000 units of ILT-101 (human recombinant IL-2; ILTOO Pharma) during 5 consecutive days and compared with an injection of PBS.

Cytometry profiling. Cells were collected from NOD Foxp3 GFP mice. Blood was submitted to RBC lysis. Pancreas was digested with collagenase/DNase solution and filtered as previously described (49). Lamina propria cells were obtained with the Lamina Propria Dissociation kit and the GentleMACS Octo Dissociator with heaters (Miltenyi Biotec). For lamina propria, a Percoll density gradient step was performed as previously described (49). We used the following monoclonal antibodies at predetermined optimal dilutions for 20 minutes at 4°C: Live Dead eFluor 780 (Thermo Fisher Scientific; catalog 65-0865-18), CD3 eFluor 450 (Thermo Fisher Scientific; clone 17A2; catalog 48-0032-82), CD8 Super Bright 600 (Thermo Fisher Scientific; clone RPA-T8; catalog 63-0088-42), CD4 Horizon v500 (BD Biosciences; clone RM4-5; catalog 560782), CD45 PE-CF594 (BD Biosciences; clone 30-F11; catalog 562420), and NKp46 Alexa Fluor 700 (BD Biosciences; clone 29A1.4; catalog 561169). Cells were acquired on a Cytoflex LX flow cytometer (Beckman Coulter) and analyzed using FlowJo software. Tregs were defined as GFP^+ cells among $CD4^+$ cells.

Monitoring of diabetes in NOD mice. Urinary glucose was measured every 2 days using colorimetric strips (Multistix, Bayer), and blood glucose was quantified by a glucometer (Optium Xceed, Abbott Diabetes Care). NOD mice were considered diabetic after 2 consecutive blood glucose readings above 250 mg/dL. In our laboratory conditions, there is no reversal of diabetes after 2 such consecutive hyperglycemic readings (49), and mice have the classic accompanying histology of islet destruction. Note that the incidence of diabetes in NOD mice is known to vary depending on the cleanliness of the animal facilities.

Induction and monitoring of DSS-induced colitis in C57BL/6J mice. DSS was added to drinking water on day 0 (50). We used a concentration of 2% DSS in water. Mice were monitored 3 times a week for body weight, stool consistency, and the presence of blood in the stool (disease activity index assessment).

FMT. Before FMT, female mice were orally gavage-fed with 200 μL of a combination of metronidazole (1 g/L), vancomycin (500 mg/L), ampicillin (1 g/L), and neomycin sulfate (1 g/L) in sterile water for 14 days as previously described (51, 52). Then, 200 mg of fresh stool (10 pellets) was suspended in 50 volumes of sterile water (1 mL) and 400 μL of this suspension was given to each recipient mouse by oral gavage using a 24G round tip gavage needle, for 2 consecutive days (53).

Mouse fecal DNA extraction and 16S rRNA gene sequencing. Mouse fecal genomic DNA was extracted and 16S rRNA sequenced as previously described (54).

Processing of 16S rRNA gene sequencing data. Raw-read quality filtering was performed with the PRINSEQ-lite (55) using a Phred quality threshold of 30. Paired-end reads were assembled using FLASH with a minimum overlap of 30 bases and a 97% overlap identity (56). Finally, CutAdapt was used to remove both forward and reverse primer sequences, with no mismatches allowed in those sequences (57).

Analysis of 16S rRNA sequencing data. Microbiota profiles were analyzed using QIIME2 based on the SILVA (release 132) database (58). Taxa with a cumulated abundance lower than 0.01% in the whole data set were filtered out. Differentially abundant taxa were identified using a sparse partial least-squares discriminant analysis (sPLS-DA) approach with a feature selection based on an effect size for the Wilcoxon signed-rank test higher than 0.5.

Collection of human samples. Six patients from the TRANSREG trial (ClinicalTrials.gov NCT01988506) (27) (2 with Sjögren's disease, 1 with Crohn's disease, 1 with Behçet's disease, 1 with psoriasis, and 1 with systemic sclerosis) had available feces samples collected at baseline and between 3 and 6 months after the first $IL-2_{LD}$ injection.

Human and mouse fecal metagenomic profiling. Total fecal DNA was shotgun-sequenced using ion-proton technology (Thermo Fisher Scientific), resulting in 23.7 ± 0.8 million (mean ± SD) single-end short reads of 150 bases as a mean. Each sample produced at least 20 million single-end DNA reads from 45 to 370 bp.

Processing of metagenomic sequencing data. Raw reads were cleaned using AlienTrimmer to remove resilient sequencing adapters and low-quality bases (59). Reads were filtered from human DNA and other possible food contaminant DNA (using *Homo sapiens*, *Bos taurus*, and *Arabidopsis thaliana* assemblies and an identity score threshold of 97%). Reads with a length less than 100 bp were removed.

Analysis of metagenomic sequencing data. MetaPhlAn2 and HUMAnN2 were used to assess the relative abundance of microbial communities and microbial pathways (60, 61). Taxa with an accumulated abundance lower than 0.01% in the whole data set were filtered out. Species and pathways differentially abundant between conditions were identified using an sPLS-DA approach (62). Prior to the discriminant

analysis, a feature selection was performed to select species and pathways with an effect size for a Wilcoxon signed-rank test higher than 0.5 for patients.

Confirmatory principal component analysis of mouse metagenomic profiles. The confirmatory principal component analysis was generated as described below. A gut microbiome gene catalog was built using bacterial genes extracted from proprietary Illumina sequencing data of the gut microbiome from selected mouse strains (HDDR1, Taconix, BALB/c, and C57BL/6J) and the Illumina sequencing data from the public mouse microbiome gene catalog (63). This gut microbiome gene catalog was built by performing metagenomic assembly using MegaHit (v1.1.2) followed by gene prediction using GeneMark-HM (64) and by clustering all the gene sequences at 95% identity over 90% length coverage using CD-HIT (v4.7). All the sequencing data used for these steps were mapped back on the microbiome gene catalog using BBmap, retaining only reads aligned with at least 95% identity and with a minimum length of 45 nucleotides. An abundance table was derived using the raw-read counts of each gene. This abundance information was used by MSPminer to generate 761 metagenomic species pangenomes (MSPs) (65).

High-quality sequencing data from the mouse strains analyzed in the present work were aligned against this newly constructed mouse gut microbiome gene catalog using BBmap with the same parameters as described above. Raw-read gene counts were normalized by the gene length and scaled by the total number of reads per sample to generate relative abundance values for each gene. MSP abundances were calculated by summing all the relative abundances of each gene belonging to a particular MSP and analyzed using R (v3.5) to perform the different statistical analyses. Principal component analysis was performed using the centered and scaled abundance values of the MSPs that were present in at least 70% of the samples (674 MSPs for NOD mice and 643 MSPs for C57BL/6J mice), using the prcomp function.

Data and materials availability. 16S rRNA gene sequencing and shotgun metagenomics sequencing data have been deposited in NCBI's Sequence Read Archive (SRA) database and are available through the accession number PRJNA831236.

Statistics. The 2-tailed Student's *t* test was used to compare body weight variation, disease activity, and Treg abundance in treated and control mice at each time point. The χ^2 test was used to compare the Kaplan-Meier estimators. The Holm-Bonferroni adjustment was used for multiple-comparison correction. A *P* value less than 0.05 was considered significant.

Study approval. All animal procedures were approved by the Regional Ethics Committee on Animal Experimentation No. 5 of the Ile-de-France region (Ce5/2012/031). All participants provided written informed consent to participate in the study. The human study was approved by the IRB of the Pitié-Salpêtrière Hospital (CPP-IdFVI) and performed in accordance with the Declaration of Helsinki and good clinical practice.

Author contributions

DK contributed to the study concept, supervision, and funding. JC, GC, and GF conducted mouse experiments. TWH and HS performed 16S rRNA sequencing. ELC and SDE conducted metagenomics shotgun sequencing. All authors contributed to data analysis. NT, ONT, GP, SD, and DK wrote the manuscript. FS, CG, and CB performed the confirmatory principal component analysis of mouse metagenomic profiles. All authors revised the manuscript and approved its final version.

1. Sakaguchi S, et al. Foxp3+ CD25+ CD4+ natural regulatory T cells in dominant self-tolerance and autoimmune disease. *Immunol Rev*. 2006;212:8–27.
2. Klatzmann D, Abbas AK. The promise of low-dose interleukin-2 therapy for autoimmune and inflammatory diseases. *Nat Rev Immunol*. 2015;15(5):283–294.

3. Liao W, et al. Interleukin-2 at the crossroads of effector responses, tolerance, and immunotherapy. *Immunity*. 2013;38(1):13–25.

4. Ritvo P-GG, et al. T$_{fr}$ cells lack IL-2Rα but express decoy IL-1R2 and IL-1Ra and suppress the IL-1-dependent activation of T$_{fh}$ cells. *Sci Immunol*. 2017;2(15):eaan0368.

5. Sakaguchi S, et al. Regulatory T cells and immune tolerance. *Cell*. 2008;133(5):775–787.

6. Burzyn D, et al. A special population of regulatory T cells potentiates muscle repair. *Cell*. 2013;155(6):1282–1295.

7. Tremaroli V, Bäckhed F. Functional interactions between the gut microbiota and host metabolism. *Nature*. 2012;489(7415):242–249.

8. Clemente JC, et al. The role of the gut microbiome in systemic inflammatory disease. *BMJ*. 2018;360:j5145.

9. Erdman SE, et al. CD4+ CD25+ regulatory T lymphocytes inhibit microbially induced colon cancer in Rag2-deficient mice. *Am J Pathol*. 2003;162(2):691–702.

10. Ishikawa H, et al. Effect of intestinal microbiota on the induction of regulatory CD25+ CD4+ T cells. *Clin Exp Immunol*. 2008;153(1):127–135.

11. Maslowski KM, Mackay CR. Diet, gut microbiota and immune responses. *Nat Immunol*. 2011;12(1):5–9.

12. Vatanen T, et al. Variation in microbiome LPS immunogenicity contributes to autoimmunity in humans. *Cell*. 2016;165(6):1551.

13. Yassour M, et al. Natural history of the infant gut microbiome and impact of antibiotic treatment on bacterial strain diversity and stability. *Sci Transl Med*. 2016;8(343):343ra81.

14. Kosiewicz MM, et al. Relationship between gut microbiota and development of T cell associated disease. *FEBS Lett*. 2014;588(22):4195–4206.

15. Willing BP, et al. Shifting the balance: antibiotic effects on host-microbiota mutualism. *Nat Rev Microbiol*. 2011;9(4):233–243.

16. Round JL, Mazmanian SK. Inducible Foxp3+ regulatory T-cell development by a commensal bacterium of the intestinal microbiota. *Proc Natl Acad Sci U S A*. 2010;107(27):12204–12209.

17. Cording S, et al. Commensal microbiota drive proliferation of conventional and Foxp3(+) regulatory CD4(+) T cells in mesenteric lymph nodes and Peyer's patches. *Eur J Microbiol Immunol (Bp)*. 2013;3(1):1–10.

18. Geuking MB, et al. Intestinal bacterial colonization induces mutualistic regulatory T cell responses. *Immunity*. 2011;34(5):794–806.

19. Smith PM, et al. The microbial metabolites, short-chain fatty acids, regulate colonic Treg cell homeostasis. *Science*. 2013;341(6145):569–573.

20. Panduro M, et al. Tissue Tregs. *Annu Rev Immunol*. 2016;34:609–633.

21. Tanoue T, et al. Development and maintenance of intestinal regulatory T cells. *Nat Rev Immunol*. 2016;16(5):295–309.

22. Goettel JA, et al. Low-dose interleukin-2 ameliorates colitis in a preclinical humanized mouse model. *Cell Mol Gastroenterol Hepatol*. 2019;8(2):193–195.

23. Mullaney JA, et al. Type 1 diabetes susceptibility alleles are associated with distinct alterations in the gut microbiota. *Microbiome*. 2018;6(1):35.

24. Churlaud G, et al. Sustained stimulation and expansion of Tregs by IL2 control autoimmunity without impairing immune responses to infection, vaccination and cancer. *Clin Immunol*. 2014;151(2):114–126.

25. Yamanouchi J, et al. Interleukin-2 gene variation impairs regulatory T cell function and causes autoimmunity. *Nat Genet*. 2007;39(3):329–337.

26. Benoit G, et al. Multiple comparative metagenomics using multiset k-mer counting. *PeerJ Comp Sci*. 2016;2:e94.

27. Rosenzwajg M, et al. Immunological and clinical effects of low-dose interleukin-2 across 11 autoimmune diseases in a single, open clinical trial. *Ann Rheum Dis*. 2019;78(2):209–217.

28. Zegarra-Ruiz DF, et al. Thymic development of gut-microbiota-specific T cells. *Nature*. 2021;594(7863):413–417.

29. Regen T, et al. IL-17 controls central nervous system autoimmunity through the intestinal microbiome. *Sci Immunol*. 2021;6(56):eaaz6563.

30. Iida N, et al. Commensal bacteria control cancer response to therapy by modulating the tumor microenvironment. *Science*. 2013;342(6161):967–970.

31. Viaud S, et al. The intestinal microbiota modulates the anticancer immune effects of cyclophosphamide. *Science*. 2013;342(6161):971–976.

32. Gopalakrishnan V, et al. Gut microbiome modulates response to anti-PD-1 immunotherapy in melanoma patients. *Science*. 2018;359(6371):97–103.

33. Boyman O, et al. Selective stimulation of T cell subsets with antibody-cytokine immune complexes. *Science*. 2006;311(5769):1924–1927.

34. Lin C-H, Hünig T. Efficient expansion of regulatory T cells in vitro and in vivo with a CD28 superagonist. *Eur J Immunol*. 2003;33(3):626–638.

35. Qi C-J, et al. Imbalance of fecal microbiota at newly diagnosed type 1 diabetes in Chinese children. *Chin Med J (Engl)*. 2016;129(11):1298–1304.

36. Sokol H, et al. Faecalibacterium prausnitzii is an anti-inflammatory commensal bacterium identified by gut microbiota analysis of Crohn disease patients. *Proc Natl Acad Sci U S A*. 2008;105(43):16731–16736.

37. Furusawa Y, et al. Commensal microbe-derived butyrate induces the differentiation of colonic regulatory T cells. *Nature*. 2013;504(7480):446–450.

38. Bui TPN, et al. Comparative genomics and physiology of the butyrate-producing bacterium Intestinimonas butyriciproducens. *Environ Microbiol Rep*. 2016;8(6):1024–1037.

39. Bui TPN, et al. Intestinimonas-like bacteria are important butyrate producers that utilize Nε-fructosyllysine and lysine in formula-fed infants and adults. *J Funct Foods*. 2020;70:103974.

40. Bian X, et al. Administration of *Akkermansia muciniphila* ameliorates dextran sulfate sodium-induced ulcerative colitis in mice. *Front Microbiol*. 2019;10:2259.

41. Hänninen A, et al. *Akkermansia muciniphila* induces gut microbiota remodelling and controls islet autoimmunity in NOD mice. *Gut*. 2018;67(8):1445–1453.

42. Ansaldo E, et al. *Akkermansia muciniphila* induces intestinal adaptive immune responses during homeostasis. *Science*. 2019;364(6446):1179–1184.

43. Rowan F, et al. Desulfovibrio bacterial species are increased in ulcerative colitis. *Dis Colon Rectum*. 2010;53(11):1530–1536.

44. Sodré FMC, et al. Peptidylarginine deiminase inhibition prevents diabetes development in NOD mice. *Diabetes*. 2021;70(2):516–528.

45. Rondas D, et al. Citrullinated glucose-regulated protein 78 is an autoantigen in type 1 diabetes. *Diabetes*. 2015;64(2):573–586.

46. Buitinga M, et al. Inflammation-induced citrullinated glucose-regulated protein 78 elicits immune responses in human type 1 diabetes. *Diabetes*. 2018;67(11):2337–2348.

47. de Groot P, et al. Faecal microbiota transplantation halts progression of human new-onset type 1 diabetes in a randomised controlled trial. *Gut*. 2021;70(1):92–105.

48. Wang S, et al. MyD88 adaptor-dependent microbial sensing by regulatory T cells promotes mucosal tolerance and enforces commensalism. *Immunity*. 2015;43(2):289–303.

49. Grinberg-Bleyer Y, et al. IL-2 reverses established type 1 diabetes in NOD mice by a local effect on pancreatic regulatory T cells. *J Exp Med*. 2010;207(9):1871–1878.

50. Chassaing B, et al. Dextran sulfate sodium (DSS)-induced colitis in mice. *Curr Protoc Immunol*. 2014;104:15.25.1–15.25.14.

51. Ghosh S, et al. Colonic microbiota alters host susceptibility to infectious colitis by modulating inflammation, redox status, and ion transporter gene expression. *Am J Physiol Gastrointest Liver Physiol*. 2011;301(1):G39–G49.

52. Brown K, et al. Prolonged antibiotic treatment induces a diabetogenic intestinal microbiome that accelerates diabetes in NOD mice. *ISME J*. 2016;10(2):321–332.

53. Markle JGM, et al. Sex differences in the gut microbiome drive hormone-dependent regulation of autoimmunity. *Science*. 2013;339(6123):1084–1088.

54. Lamas B, et al. CARD9 impacts colitis by altering gut microbiota metabolism of tryptophan into aryl hydrocarbon receptor ligands. *Nat Med*. 2016;22(6):598–605.

55. Schmieder R, Edwards R. Quality control and preprocessing of metagenomic datasets. *Bioinformatics*. 2011;27(6):863–864.

56. Magoc T, Salzberg SL. FLASH: fast length adjustment of short reads to improve genome assemblies. *Bioinformatics*. 2011;27(21):2957–2963.

57. Martin M. Cutadapt removes adapter sequences from high-throughput sequencing reads. *EMBnet journal*. 2011;17(1):10–12.

58. Bolyen E, et al. Reproducible, interactive, scalable and extensible microbiome data science using QIIME 2. *Nat Biotechnol*. 2019;37(8):852–857.

59. Criscuolo A, Brisse S. AlienTrimmer: a tool to quickly and accurately trim off multiple short contaminant sequences from high-throughput sequencing reads. *Genomics*. 2013;102(5–6):500–506.

60. Truong DT, et al. MetaPhlAn2 for enhanced metagenomic taxonomic profiling. *Nat Methods*. 2015;12(10):902–903.

61. Franzosa EA, et al. Species-level functional profiling of metagenomes and metatranscriptomes. *Nat Methods*. 2018;15(11):962–968.

62. Lê Cao KA, et al. Sparse PLS discriminant analysis: biologically relevant feature selection and graphical displays for multiclass problems. *BMC Bioinformatics*. 2011;12(1):253.

63. Lesker TR, et al. An integrated metagenome catalog reveals new insights into the murine gut microbiome. *Cell Rep*. 2020;30(9):2909–2922.

64. Lomsadze A, et al. GeneMark-HM: improving gene prediction in DNA sequences of human microbiome. *NAR Genom Bioinform*. 2021;3(2):10.

65. Plaza Oñate F, et al. MSPminer: abundance-based reconstitution of microbial pan-genomes from shotgun metagenomic data. *Bioinformatics*. 2019;35(9):1544–1552.